# Magnetic Field Orientation of Liquid Crystalline Epoxy Thermosets

**Brian C. Benicewicz[†] and Mark E. Smith**

*Polymers and Coatings Group, Los Alamos National Laboratory, Los Alamos, New Mexico 87545*

**Jim D. Earls and Ralph D. Priester, Jr.**

*The Dow Chemical Company, Freeport, Texas 77541*

**Stefan M. Setz,[‡] Randolph S. Duran,[‡] and Elliot P. Douglas*[,§]**

*Departments of Chemistry and Materials Science and Engineering, University of Florida, Gainesville, Florida 32611*

*Received January 20, 1998; Revised Manuscript Received May 21, 1998*

ABSTRACT: The effect of magnetic fields on the orientation and properties of 4,4′-bis(2,3-epoxypropoxy)-α-methylstilbene cured with sulfanilamide has been studied. This epoxy system is initially isotropic and forms a smectic A phase upon curing. A magnetic field was applied during the cure reaction, resulting in alignment of the molecules along the direction of the applied field. Measurement of the orientation parameter of the fully cured material by wide-angle X-ray scattering (WAXS) showed that orientation improved with an increase in field strength. The orientation parameters of the smectic layer normals calculated from the inner reflection of the WAXS pattern attained a maximum level of approximately 0.8 at a field strength of approximately 12 T. The orientation parameters calculated from the outer reflection of the WAXS pattern were considerably lower, possibly due to the presence of amorphous regions associated with domain boundaries or the loss of molecular alignment within the smectic layers due to topological restrictions of the cross-linking sites. Orientation resulted in an anisotropic linear thermal expansion coefficient after curing, although the overall volumetric expansion was constant. The elastic tensile modulus increased with the square of the orientation parameter, attaining a maximum value of 8.1 GPa, compared to 3.1 GPa for the unoriented material. The change in modulus with orientation could be fit with a simple model for the modulus of anisotropic materials.

## Introduction

The development of high performance polymers for structural applications has been driven by the ability to create anisotropy at the molecular level in order to obtain superior mechanical properties. Fibers based on polyaramid and polyester liquid crystals owe their exceptional tensile properties to the high degree of molecular alignment caused by extensional flow during fiber spinning. Unfortunately, the use of flow fields poses some limitations on the types of materials that can be made. Because of the high viscosity of polymers, flow fields are only effective for certain geometries and, generally, for small structures such as fibers. For example, in injection molding of liquid crystalline polyesters only a thin outer skin is oriented, leaving an unoriented inner core;[1] improvements in tensile properties for injection molded parts are significantly less than what could be achieved in the case of complete bulk orientation. Thus, approaches are required which result in improved orientation throughout the bulk of a thick sample.

The use of magnetic fields for processing of polymeric materials remains an area of great promise and has the potential to fill the need described above. Magnetic fields are fundamentally different from flow in that the effective field strength does not decrease in the center of the sample. Magnetic field effects on polymers are well-known, and a number of publications and reviews describe the use of magnetic fields to orient polymers.[2−20] In almost every case the materials of interest have been liquid crystals. The cooperative nature of molecular motions in a liquid crystalline phase is required to obtain orientation at realistic field strengths. The effects studied include the Fredericks transition,[21] the liquid crystal defect structure,[22−24] determination of the Frank elastic constants,[24] and the mechanism and kinetics of the orientation process.[25−29]

There have been only a few studies that have examined physical properties of polymers oriented in magnetic fields.[30−32] Of particular note are the studies involving liquid crystalline thermosets (LCT's). LCT's are generally defined as low molar mass liquid crystals to which cross-linkable endgroups are attached. These molecules can then be reacted thermally, chemically, or photochemically to give a cross-linked solid with liquid crystalline order. Several publications describe the physical properties of both unoriented and oriented LCT's. Among the properties studied are the linear viscoelastic properties,[33−37] stress−strain behavior in the rubbery phase,[38] fracture toughness,[39,40] and dielectric properties.[41] Several research groups have shown that LCT's can be oriented by curing in a magnetic field[33,42−44] and that the resulting materials have an anisotropic coefficient of thermal expansion.[30] Of particular interest to our work are the studies by Ober and co-workers.[31,32] They have examined the orientation of a series of epoxy monomers, oligoethers of dihydroxy-α-methylstilbene, cured in a 13.5 T magnetic field.

* To whom correspondence should be addressed.
[†] Current address: Department of Chemistry and Center for Polymer Synthesis, Rensselaer Polytechnic Institute, Troy, NY 12180.
[‡] Department of Chemistry.
[§] Department of Materials Science and Engineering.

S0024-9297(98)00058-8 CCC: $15.00 
Published on Web 07/10/1998

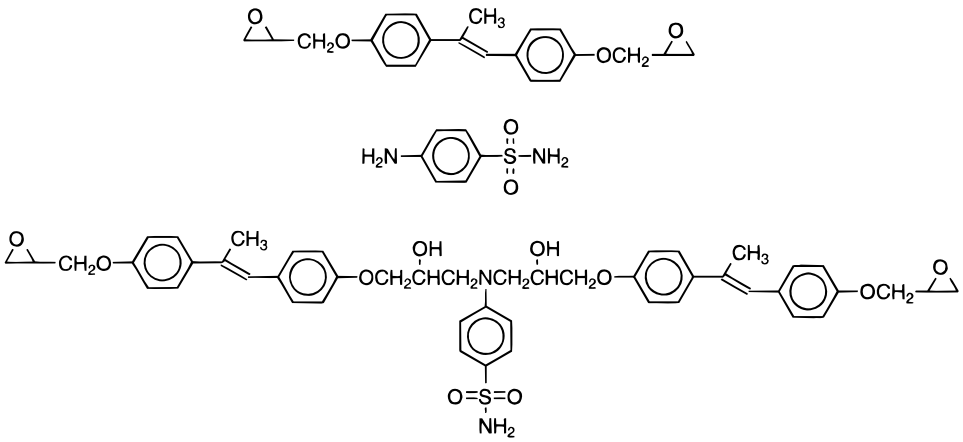

**Figure 1.** Structures for EPAMS (top), sulfanilamide (middle), and one type of cross-linking point (bottom).

Their results show that the level of orientation depends on the length of the oligomer.

Our goal is to investigate the effects of magnetic fields on the mechanical properties of LCT's under static loading conditions. We report here our results for a specific epoxy monomer, 4,4′-bis(2,3-epoxypropoxy)-α-methylstilbene cured with sulfanilamide. Structures for these materials are shown in Figure 1. Specifically, we have measured the macroscopic orientation induced in this LCT by magnetic fields using wide-angle X-ray scattering (WAXS). The influence of this macroscopic orientation on the thermal expansion and tensile modulus is then described. The results provide an initial understanding of how magnetic fields can be used to control the bulk physical properties of LCT's.

## Experimental Section

**Materials.** 4,4′-Bis(2,3-epoxypropoxy)-α-methylstilbene (EPAMS) was synthesized as described previously.[45] The resulting EPAMS contains approximately 10% of a tetrafunctional dimer and was used without further purification. Sulfanilamide (SAA) was purchased from Aldrich Chemical Co. and used as received. The organophosphonium catalyst was obtained from The Dow Chemical Co.

**Magnetic Field Processing.** The thermoset formulation was prepared by dissolving 1 equiv of SAA into 1 equiv of EPAMS at 150 °C, which corresponds to a stoichiometric equivalence of reactive sites. The temperature was then lowered to 120 °C, 2 mequiv of an organophosphonium catalyst was added, and the mixture was degassed under a mild vacuum. The thermoset formulation was then poured into a mold for the magnetic field experiments. This mold consisted of a Teflon cup into which were placed two aluminum heater blocks, with the thermoset formulation filling the space between the blocks. Temperature control was maintained with a PID controller. Magnetic field experiments were conducted at the National High Magnetic Field Laboratory using a variable field resistive magnet. Curing was done in the field for 1 h at 150 °C. The sample was then removed from the mold by cutting the Teflon cup and separating the aluminum plates. The final cure was done in a conventional oven, and consisted of an additional 3 h at 150 °C, 1 h at 175 °C, and 4 h at 200 °C. This is a standard cure cycle for epoxy resins. Differential scanning calorimetry of unoriented samples subjected to the full cure cycle do not exhibit any residual cure exotherm, indicating that the samples are fully cured. All samples were opaque and off-white, similar in appearance to the uncured formulation. Plaques approximately 2 in. × 1.5 in. × 0.125 in. were obtained. Samples are designated as T*x*, where *x* is the magnetic field strength.

**Thermal Expansion.** Thermal expansion measurements were performed parallel and perpendicular to the field direction using an Omnitherm TMA 1000 with a heating rate of 5 °C/min and a mass of 10 g. Values of CTE reported are calculated by a linear fit of the displacement-temperature curve over the temperature range 30−60 °C.

**Tensile Properties.** Tensile properties were measured on ASTM D638 Type V tensile specimens using an Instron 4483 testing machine with a 9 kN load cell. Extension of the samples was measured with an MTS 632.26E extensometer with a gauge length of 8 mm. Samples were strained at a crosshead speed of 5 mm/min. Self-tightening grips with serrated faces were used to prevent slippage of the samples in the grips. Tensile modulus was determined as the initial slope of the engineering stress vs strain curve. The data reported represent the average of at least three samples cut from the same plaque.

**Wide-Angle X-ray Scattering (WAXS).** WAXS patterns were collected in transmission using point collimated, monochromatic Cu Kα radiation on a Bruker platform goniometer. The source of the beam was a Kristalloflex 760 2.2 kW generator and long fine focus tube equipped with cross coupled Göble mirror monochromator and 300 $\mu$m collimation. An additional 300 $\mu$m pinhole was pressed against the specimen in a transmission sample holder to further reduce noise from edge scatter. A HI−STAR area detector was mounted for data collection at 10 cm distance from the sample. Samples of 0.75−1.5 mm thickness were exposed for 7752 s. A 4° beam stop was mounted 40 mm behind the specimen. Data were processed with the GADDS program. The data were unwarped for inhomogeneous response in the flood field of the detector. A measurement using the empty camera under the same conditions was used for background correction, taking the specimen absorption at the primary beam into account.

Absorption of the material was measured from 9 specimens of the T3 material, with thicknesses between 0.55 and 4.15 mm. The absorption coefficient $\mu$ for the material was determined to be $10.32 \pm 0.07$ cm$^{-1}$ using the Lambert−Beer law in the natural logarithmic form.

During these experiments no measurable anomalous scattering was observed in the small angle range up to $2\theta = 2°$. GADDS program data normalization routines that include absorption of the specimen, air, and detector face plate were applied to the data sets. Four examples of the fully corrected scattering patterns are given in Figure 2.

The azimuthal intensity distribution $I(\chi)$ for the two reflections were evaluated by integration in a radial step size of 0.1 deg through the whole circle. Intensities were integrated along $2\theta$ from $2\theta = 3.2$ to $2\theta = 5.4°$ for the inner reflection, and from $2\theta = 9.6$ to $2\theta = 24.0°$ for the outer reflection. To correct for amorphous scattering in the area of the inner reflection, integrals from $2\theta = 2.9$ to $2\theta = 3.2°$ and $2\theta = 5.4$ to $2\theta = 5.7°$ were taken as well and their averaged intensities subtracted from the previous results. Due to the sharpness and intensity of the inner reflection, we could assume a linear baseline. However, this baseline correction could not be performed for the outer reflection because it consists of two diffuse peaks, likely centered at 4.5 and 5.7 Å. (see Figure 3). Thus, in the

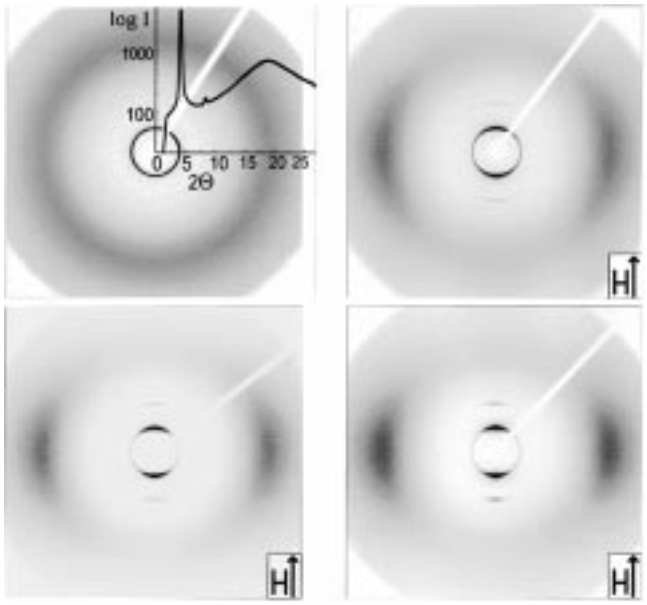


**Figure 2.** Intensity distribution of WAXS measurement depicted on a logarithmic gray scale in order to show all reflections at the same time. The arrow in the lower right corner indicates the direction of the magnetic field during the curing. The azimuthal intensity distribution of the inner ring at $2\theta = 4.14° \pm 0.05°$ was used to determine the orientation parameter. The width of the detector face plate is 24.4°. The pattern is typical for smectic A liquid crystals. Top left, T0; top right, T3; bottom left, T9; bottom right, T18. The inset for T0 gives the intensity of a radial scan.

absence of any physical model for the scattering in this region, the data for the outer reflection were left uncorrected for a baseline. The data were transferred into a spreadsheet program and the two peaks in each plot were averaged and the shadow of the beam stop removed. To compensate for vertical misalignment of the specimen the data were shifted by up to 2° to achieve maximum intensities on the azimuth at $\chi = 0°$ for the inner reflection and on the equator at $\chi = 90°$ for the outer reflection. Counts at positive $\chi$ were averaged with those at negative $\chi$. The intensity distribution in the sample $I(\alpha)$ was then determined from the azimuthal intensity distribution $I(\chi)$ by

$$\cos \alpha = \cos \chi \cos \theta \tag{1}$$

where $\theta$ is the Bragg angle for the scattering peak and $\alpha$ is the angle between the normal to the scattering planes and the magnetic field direction. This transformation results in no experimental data being available for $\alpha$ from 0° to $\theta$, and so the data were extrapolated to provide intensity values over the entire range from $\alpha = 0°$ to $\alpha = 90°$. The data for the outer reflection were then shifted to provide the maximum peak intensity at 0°. This was done for convenience in interpreting the data in terms of the orientation of the molecular axis with respect to the field direction.

From the intensity distribution $I(\alpha)$, the average cosine squared of the angle with respect to the field direction was determined according to

$$\langle \cos^2 \alpha \rangle = \frac{\int_0^{\pi/2} I(\alpha) \sin \alpha \cos^2 \alpha \, d\alpha}{\int_0^{\pi/2} I(\alpha) \sin \alpha \, d\alpha} \tag{2}$$

and the second moment of the orientation function was determined according to

$$S = \frac{1}{2}(3\langle \cos^2 \alpha \rangle - 1) \tag{3}$$

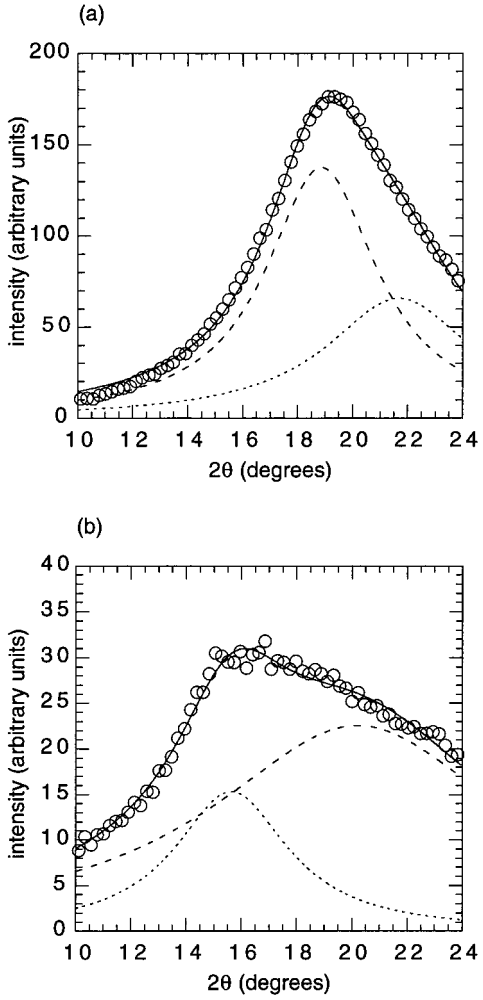


**Figure 3.** Scattering in the vicinity of the outer reflection along the (a) equatorial and (b) azimuthal directions for T18. Dashed lines are single Lorentzian peak fits to the data, the solid line is the sum of the fitted peaks, and the points are the experimental data. For clarity, not all data points are shown.

For comparison to the orientation parameters calculated from the two-dimensional WAXS patterns, complete pole figures for the sample prepared at 9 T were determined. The pole figures for both reflections were prepared by collecting 24 different exposures of 1200 s duration with the sample at different orientations to the primary beam. Twelve exposures were obtained by tilting the sample in 6° steps around $\phi$ beginning at $\phi = -43.5°$ with $\omega = 0°$, and another 12 exposures were obtained by tilting the sample in 6° steps around $\omega$ beginning at $\omega = -43.5°$ with $\phi = 5°$; $\omega$ is the angle around an axis parallel to the orientation direction in the sample, and $\phi$ is the angle around an axis perpendicular to both the primary beam and the orientation direction in the sample. The different scattering patterns were corrected in the same way as the single exposures. Pole figures for the two reflections were constructed and interpolated from the 24 exposures using the GADDS software, and the orientation parameters were calculated from the pole figures using the procedures in the GADDS software.

## Results and Discussion

**Curing Behavior.** The advantages of using a thermoset for this study stem from its low initial viscosity. A previous model for orientation of liquid crystalline polymers in a magnetic field showed that the time for orientation is a strong function of the rotational viscosity, decreasing as the rotational viscosity decreases.[29]

On the other hand, for good mechanical properties, one needs a high molecular weight material, which has an inherently high melt viscosity. The use of a thermoset system allows orientation to proceed while the material is a low viscosity liquid. Subsequent curing in the field locks in the oriented structure and provides a solid material with good mechanical integrity. However, the dynamic behavior of a reactive system results in a complicated interplay between the formation of the network structure and the orientation process. Thus, an understanding of the cure behavior is essential to understanding how the orientation process proceeds.

The EPAMS/SAA system is initially isotropic at the curing temperature of 150 °C. A smectic A phase forms after about 20 min of isothermal cure. Formation of a more ordered phase during isothermal cure has been seen previously in several studies in a variety of LCT's.[46−48] The reaction-induced isothermal phase transition can be explained in terms of the basic principles of step−growth polymerization and the packing of rod-like molecules—first described by Onsager and Flory.[49] At low conversions, the monomer population rapidly decreases and conjugates of singly substituted cross-linker and stilbene moieties rapidly form. As the cure reaction proceeds, the aspect ratio of the growing rodlike molecules increases. At some critical aspect ratio the entropic driving force for packing of rods results in the formation of an ordered phase. Of course, this explanation is clearly an oversimplification. In reality, the rods do not simply become longer, but are eventually reacted into a cross-linked network structure. Thus, the details of the formation of an ordered phase during cure will depend on how the network structure is formed during the course of the reaction. Previous work has suggested that the formation of an ordered phase during cure is enhanced by using a diamine in which the two amine groups have unequal reactivity,[50] as is the case for SAA. This would then allow a substantial amount of chain extension to occur prior to branching and eventual cross-linking.

The phase change during cure is important to achieve macroscopic orientation at realistic field strengths. It is generally recognized that an ordered phase is required for orientation to occur at reasonably achievable field strengths.[51] The driving force for orientation in an organic molecule is the anisotropy in its diamagnetic susceptibility. For an isolated molecule in the gas phase, or equivalently a molecule in the isotropic melt, the energy decrease due to orientation is generally orders of magnitude less than the thermal energy. In contrast, in a condensed ordered phase like a liquid crystal the molecular motions are cooperative, and thus the total energy decrease is given by the energy decrease for a single molecule multiplied by the number of molecules present. In large samples, macroscopic orientation can be achieved. As a consequence of this effect, we have chosen a cure time that is well beyond the time required to form a liquid crystalline phase.

The other important consideration for our experiments is the gel time. It is desirable to cure in the magnetic field long enough to lock in the macroscopic orientation, as well as to minimize the time needed in the magnetic field for experimental purposes. The gel time is the key parameter that defines when the individual molecules are locked into the network and can no longer macroscopically relax from those positions. At 150 °C the gel time as measured rheologically from the crossover in $G'$ and $G''$ is 35 min. Thus, the materials were cured in the magnetic field for 1 h in order to ensure that time in the magnetic field was well beyond the gel time.

**Orientation.** The alignment of calamitic, or rodlike, LC molecules is quantified as the even moments of the rodlike molecules' orientation distribution.[51] Orientation in materials is measured using physical effects that are sensitive to molecular orientation. In the literature the orientation parameters of liquid crystals, liquid crystalline polymers, and networks are measured by different techniques. Birefringence,[52,53] ESR line shape analysis,[54,55] infrared dichroism,[53,56] and polarized fluorescence can lead to comparable results when determining molecular orientation but only provide the second moment of the orientation distribution. With NMR[51] and Raman spectroscopy,[57] the fourth moment of the orientation distribution can be determined. The orientation can be observed at different length scales by applying scattering methods that measure different ranges of the scattering vector. Small-angle X-ray scattering (SAXS), small-angle neutron scattering (SANS), and light scattering probe large length scales (>10 Å) and defects;[58] wide-angle X-ray scattering (WAXS) is often used for the smaller spacings between oriented moieties. WAXS is often the preferred method to determine the molecular orientation because the orientation distribution can be obtained directly from the data. Commonly the degree of orientation derived from WAXS patterns is expressed as the second moment of the orientation distribution function; this parameter is also called the Hermann's orientation parameter.[59] It is derived from a series expansion in spherical harmonics. Also, neutron scattering allows the direct observation of the distribution function when deuterium tagged molecules are used.[60] The principles of deriving the orientation parameter from WAXS data is extensively described in the literature.[61−67] Frequently two or more methods to obtain the orientation are combined.[53,68−71] The shape and width of the distribution function can be described by higher moments of the orientation distribution.[72] This is especially necessary for LC polymers with more complex organization. A direct comparison of birefringence, WAXS and SAXS studies, and infrared (IR) dichroism on stretched HDPE is given by Yu and Wilkes.[73] The similarities and differences between the different methods were examined recently.[60] A critical overview of the influence of different orientation distributions on the orientation parameter is given by Lafrance et al.[74]

For our investigation, we have determined the orientation parameter, $S$, using WAXS. Due to cylindrical symmetry, only a quarter of the WAXS data have to be evaluated. To improve signal-to-noise ratio, it is desirable to average the four quadrants in an appropriate manner. WAXS also requires good separation of the data from the baseline. The background in the equatorial position has to be determined very carefully because the denominator in the definition of $\langle \cos^2 \alpha \rangle$ (eq 2) is very sensitive to changes in the background level. Some authors simply take the data of their sample with the highest orientation and set it as background for all specimens, and then they account for the instrumental width of the equatorial peak for a perfect aligned specimen by dividing the calculated orientation parameters by 0.97.[23,75] The brilliant, parallel X-ray beam resulting from the Göble mirror monochromator and

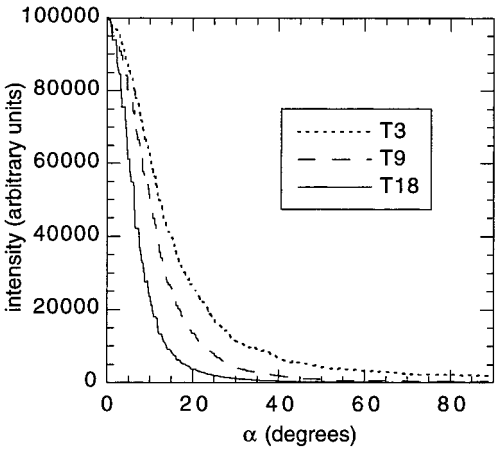


**Figure 4.** Normalized azimuthal intensity distribution for the inner reflection of three WAXS experiments.

sensitive digital detector used for this investigation results in a much finer beam and quantitative intensity information. The instrumental resolution obtained would result in an orientation parameter for a perfectly aligned specimen of higher than 0.99; consequently, such a correction was not necessary.

WAXS patterns for samples oriented at various field strengths are shown in Figure 2. Patterns consisted of two to three orders of sharp reflections in the small angle region (first order located at $2\theta = 4.14 \pm 0.05°$), highly oriented in a direction parallel to the applied magnetic field. This sequence of reflections corresponds to a layer periodicity with a *d* spacing of 21 Å. Previous work has shown that this reflection is consistent with the length of the EPAMS molecule without the cross-linker, suggesting that the SAA is attached as a side-group and is not a part of the smectic layer structure.[76] The *d* spacings of all of these features did not change measurably with the applied magnetic field. The mesogens and the smectic layer normals are oriented in the direction of the applied magnetic field and are formally consistent with smectic A-like ordering.

Figure 3 shows equatorial and azimuthal scans of sample T18 in the region of the outer reflection. These data were obtained by averaging 20° wide segments centered along the equatorial and azimuthal directions, respectively. The data could only be fit reasonably with two Lorentzian peaks, indicating that there are two correlation lengths that contribute to this reflection. In the azimuthal direction there is a clear maximum of a diffuse ring centered at a *d* spacing of about 5.7 Å; this distance approximately corresponds to the long axis of SAA. In the equatorial direction an oriented, though rather diffuse spot is observed at a *d* spacing of about 4.5 Å, in the range typically observed for lateral packing of stilbene-like mesogens. This reflection is also present in the azimuthal direction, although it is considerably weaker. The additional peak at 4.1 Å in the equatorial direction may simply reflect the distribution of correlation lengths for lateral packing of the mesogens. The positions of these peaks appear to shift slightly with field strength, although at this time we are not certain if this is a real effect or an artifact of the fitting procedure.

Three of the intensity distributions for the inner reflection after all the corrections and averaging calculations are depicted in Figure 4. The data show that it is not possible to set the background at $\alpha = 90°$ to a

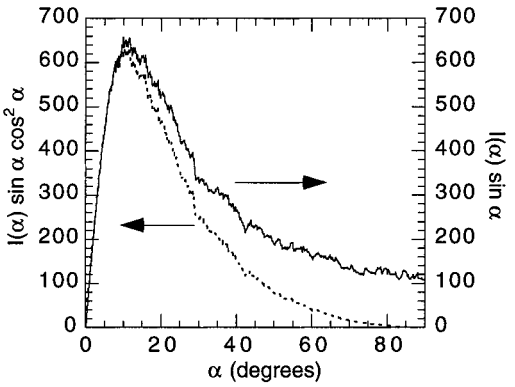


**Figure 5.** Graphical presentation of the two integrals in the ratio that determines $\langle \cos^2 \alpha \rangle$ for the lowest oriented sample T3.

common value. The shape of these peaks can be best described by a best fit using the Pearson VII function.[53]

The orientation parameter was calculated as described in the Experimental Section. An example of this calculation is given in Figure 5 for the T3 specimen. The orientation parameter is calculated from the ratio of the area under the dotted and the solid line, showing again that correct data at $\alpha = 90°$ are essential to the results. A compilation of all the measured orientation parameters is given in Figure 6. For T9 the measurement was repeated at a different location on the same specimen in order to show the reproducibility of the X-ray method. As can be seen in Figure 6, specimen T12 had a much lower orientation parameter than expected. Consequently an additional specimen T12r was fabricated and measured at a later time. Its orientation parameter fits well into the series of the other samples, although it is slightly higher than expected.

The orientation parameters for specimen T9 were also determined from the complete pole figures. Since the pole figures represent the entire distribution of scattering plane normals in space, orientation parameters calculated from them provide an independent check of the procedures used to determine orientation parameters from the two-dimensional WAXS patterns. For the inner and outer reflections, respectively, the orientation parameters determined from the pole figures are 0.76 and 0.24, in good agreement with the values of 0.73 and 0.23 calculated from the two-dimensional pattern.

The orientation parameters for the outer ring are considerably lower than those for the inner ring. There are a number of possible explanations for this behavior. Perhaps the simplest is that the rods within the layers are less ordered than the layered structure. Such a situation is possible if the alignment process occurs by rotation of entire domains or large regions, rather than individual mesogens. It is also possible that there is a liquid scattering background, which would have correlation lengths in the same range as for the liquid crystalline phase. These amorphous regions would correspond to the regions between the liquid crystalline domains. Finally, it is possible that the topology of the cross-links themselves may inhibit alignment of the mesogens within the layered structure. This effect is shown schematically in Figure 7. As mentioned above, the epoxy−amine reaction is a step-growth reaction. At short reaction times dimers and other short oligomers are the predominant species. Thus the aspect ratio of the rods doubles at low conversion, driving formation of a liquid crystalline phase and allowing

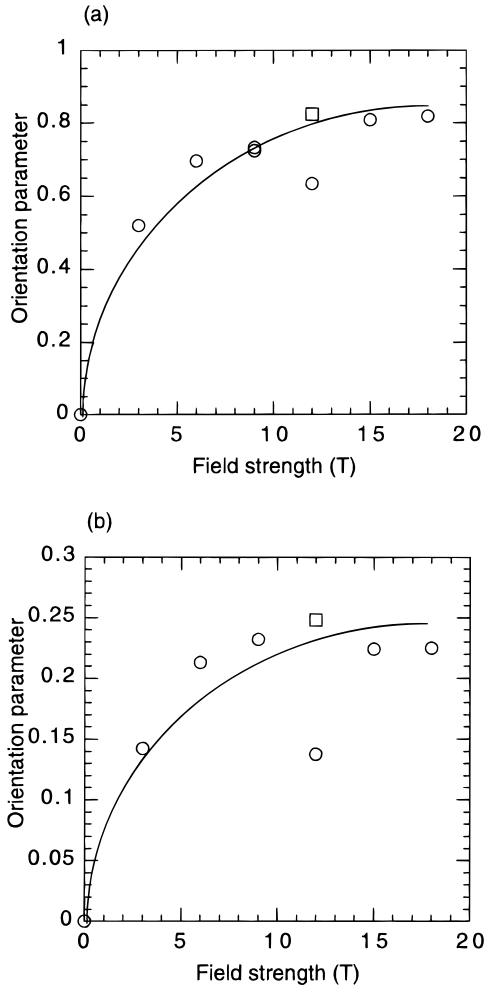


**Figure 6.** Orientation parameter calculated from WAXS data according to eqs 2 and 3 for (a) the inner reflection and (b) the outer reflection. The line is drawn to guide the eye. Square symbols are the orientation parameters for sample T12r.

alignment to occur in a magnetic field, as illustrated in Figure 7a. At higher conversion, long chains and cross-links form, and the elongated shape of the tetrafunctional amine forces local segments to become perturbed from their aligned state as the last links are made, as shown in Figure 7b. This loss of alignment may occur during the final cure outside of the magnetic field. Molecules that have not been fully cross-linked in the aligned state can be perturbed on a local level during the final cure, even though we have cured the samples in the magnetic field beyond the macroscopic gel time. A previous off-lattice Monte Carlo simulation has shown that there is a decrease in local order when liquid crystalline monomers are polymerized into a cross-linked network.[77]

The end result is that while all of the inner ring scattering is due to the smectic A layers, some of the outer ring scattering is due to mesogens well-aligned within the smectic A domains and some is due to less ordered regions caused by any one or several of the scenarios described above. We have no physical model on which to separate out these factors and identify the orientation due solely to alignment in the magnetic field. Thus, the calculated orientation parameters for the outer reflection represent the combination of these effects and are lower than the values calculated for the inner reflection. Future work is planned to measure the kinetics of the orientation process in order to determine

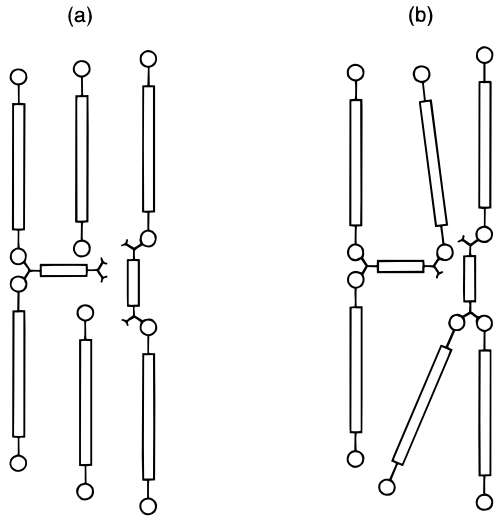


**Figure 7.** Schematic diagram of the effect of the cross-links on local orientation. The difunctional epoxy is represented by rectangles capped with circles, and the tetrafunctional diamine is represented by rectangles capped with arcs. In part a the network is partially cured, and the molecules are fully aligned. In part b, additional cross-linking perturbs the orientation of the molecules within the layers, although the orientation of the layers themselves is unaffected.

the relative contribution of each of these effects and to understand how the cross-linking reaction affects the evolution of macroscopic order in LCT's.

In the next section we are interested in correlating the physical properties with the degree of orientation. As described below, we have found that the physical properties do not correlate with orientation parameters from the outer reflection. Since the orientation represented by the outer ring is a combination of several factors which cannot be separated at this time, the properties will only be discussed in terms of the orientation parameter calculated from the inner ring.

It is useful to compare our results to other studies on orientation of LCT's. Barclay et al. have examined the orientation behavior of EPAMS and oligoethers of dihydroxy-α-methylstilbene cured with methylene dianiline (MDA) using both mechanical orientation and magnetic fields.[31,32] At low cross-link densities the oligoethers could be effectively oriented by mechanical stretching, but stretching was ineffective for EPAMS due to the very high cross-link density. Curing EPAMS in a 13.5 T magnetic field resulted in much lower orientation parameters than our study; they found values of 0.13 and 0.06 for the outer and inner reflections, respectively, compared to 0.23 and 0.73 at 9 T in our study. The difference is likely due to the faster reaction kinetics of MDA, which results in less time for orientation to occur prior to gelation. Hoyle and coworkers have examined thin films of mixtures of difunctional and monofunctional acrylate LCT's photopolymerized in the presence of a magnetic field.[42,44] Interestingly, they find that orientation parameters of roughly 0.5 can be obtained at field strengths of less than 1 T. This enhanced ability for orientation to occur compared to our work is due to the reduction in cross-link density caused by the presence of the monofunctional monomer. A similar effect was seen in the work by Barclay et al.[31,32] In addition, orientation of the acrylate LCT's was accomplished in the nematic phase. The lower viscosity of a nematic compared to a smectic

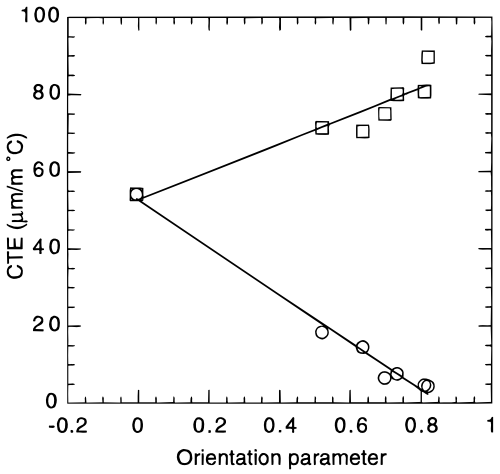


**Figure 8.** Coefficient of linear thermal expansion perpendicular and parallel to the field direction. Key: squares, perpendicular to field direction; circles, parallel to field direction. Lines are a linear fit to the data.

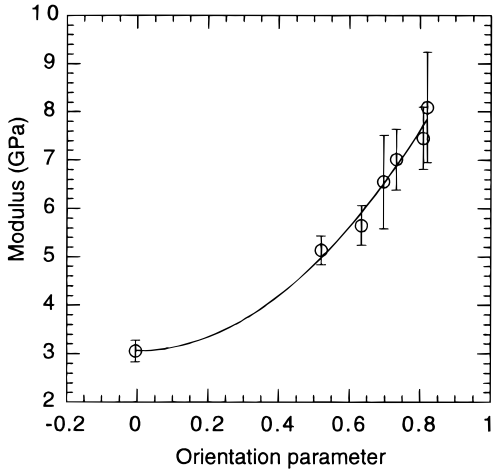


**Figure 9.** Tensile modulus as a function of the orientation parameter. The line is a quadratic fit to the data.

liquid crystal may also contribute to the higher orientation parameters compared to our work.

Other techniques can also be used to orient thin films of LCT's. Alternating current electric fields result in orientation parameters of up to 0.6, with the level and direction of orientation depending on both the applied field strength and the frequency.[78,79] Another approach is to use rubbed polyimide substrates to induce orientation.[42,44] Reasonable orientation parameters of roughly 0.5 can be obtained.

**Physical Properties.** To determine the effects of magnetic field orientation on the physical properties, the coefficient of thermal expansion (CTE) and tensile modulus were measured. To illustrate directly the effect of orientation on properties, the results are given as a function of the orientation parameter calculated from inner ring scattering data, not the field strength. As can be seen from Figures 8 and 9, the resulting curves are continuous, and thus the apparent sample variability, as evidenced by the two samples prepared at 12 T, is eliminated from consideration.

Figure 8 shows the CTE's measured both parallel and perpendicular to the field direction. As has been described previously,[30−32] the CTE parallel to the field decreases and the CTE perpendicular to the field increases as a function of orientation. In thermoplastic liquid crystals this is generally understood as being due to the difference between expansivity along the backbone (primarily covalent bonds) and perpendicular to the backbone (primarily van der Waals). However, in a cross-linked system with covalent bonds in three dimensions, such as ours, a different explanation is needed. In this case the anisotropic thermal expansion results from changes in the average areal density of covalent bonds in each direction. We assume that the cross-links primarily are formed in the space between the layers of the smectic structure. In a highly oriented system, the distance between covalent bonds in the parallel direction is a molecular diameter, while in the perpendicular direction it is the layer distance. Thus, as the material is oriented, the average areal bond density increases in the parallel direction and decreases in the perpendicular direction, resulting in an anisotropic thermal expansion. Of course, we expect the cross-links to stabilize the mesophase to far higher temperature than an analogous uncross-linked system.

Figure 8 shows linear fits to the CTE's as a function of orientation parameter; an attempted quadratic fit resulted in correlation coefficients slightly worse than for the linear fits. Using a linear fit also allows us to gain further insight into the effect of the magnetic field on this material. The slopes for the two fits are $36.2 \pm 6.2$ for the perpendicular direction and $-61.4 \pm 3.3$ for the parallel direction. Thus, within error, the parallel slope is approximately (negative) twice that of the perpendicular slope. Defining the volumetric expansion coefficient as

$$\text{CTE (volume)} = \text{CTE (parallel)} + 2*\text{CTE (perpendicular)} \quad (4)$$

we can see from the relationship between the slopes that the volumetric CTE is approximately constant, despite the orientation.

Figure 9 shows the tensile modulus as a function of the orientation parameter. The highest value for the modulus attained, 8.1 GPa, represents an increase of 2.6 times over the modulus of the unoriented sample T0, 3.1 GPa. The modulus seems to follow a quadratic dependence on the orientation parameter. Taking the orientation parameter as a measure of the average angle the director makes with the magnetic field (see eq 3), this quadratic dependence suggests that the modulus depends on $\cos^4 \alpha$. An expression with this dependence has been derived by Lees.[80] In an oriented fiber-reinforced composite, the modulus as a function of the measurement direction is given by

$$E(\alpha) = \frac{E_0 E_{90}}{E_0 - (E_0 - E_{90})(\cos^4 \alpha)} \quad (5)$$

where $\alpha$ is the angle between the fiber axis direction and the measurement direction, $E_0$ is the composite modulus in the fiber axis direction, and $E_{90}$ is the modulus in the transverse (perpendicular to the fiber) direction. It is important to note that this equation is not based on a physical model but rather is derived from performing a rotational operation on the modulus tensor. Thus, it should be valid for any anisotropic material with a smoothly varying modulus, and in fact it has been successfully used in modeling the modulus of fiber-reinforced composites,[80] semicrystalline polymers,[81] and extruded liquid crystalline polymers.[82]

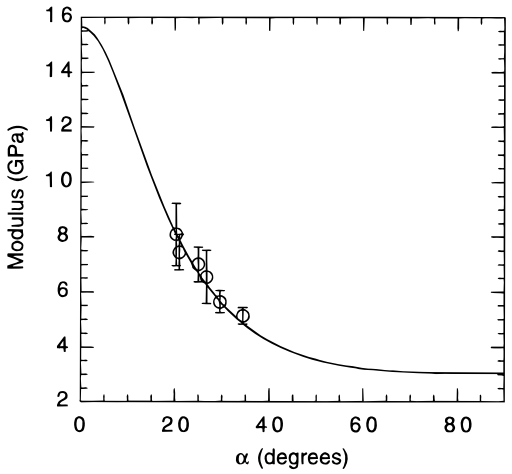


**Figure 10.** Tensile modulus as a function of the average angle α the EPAMS mesogens make with respect to the field direction. The solid line is the fit of the data according to eq 6 with $E_0 = 15.6$ GPa and $E_{90} = 3.1$ GPa.

To use this equation to model the modulus of our samples, we have taken the orientation parameters determined from WAXS and calculated the corresponding average value of $\cos^2 \alpha$ using eq 3. For $E_{90}$ we have used the modulus of the unoriented sample, which is 3.1 GPa. Previous work by us has shown that the modulus transverse to the field direction is the same as the modulus of the unoriented material.[83] The data were then fit to eq 5 using $E_0$ as a fitting parameter. The results are shown in Figure 10. Although only a limited range of data is available to us at this time, the fit is excellent. This suggests that the modulus enhancement seen in the oriented samples results from the degree of alignment of the liquid crystalline structure. A similar conclusion has been reached for oriented thermoplastic liquid crystalline polymers.[82] We did attempt to fit the modulus vs orientation data using orientation parameters from the outer reflection, and we found that the nonlinear fit diverged. This provides further evidence that the outer reflection contains contributions from mesogens that have become less ordered during the final cure and that the physical properties are controlled by the orientation of the smectic layer structure. In terms of the modulus, we assume that this indicates the controlling factor is stress transfer at the smectic layer boundaries, although more experiments would be needed to understand this point. The value of $E_0$ from the fit of the data in Figure 10 is 15.6 GPa. This value of $E_0$ does not correspond to the value expected for a single molecule. Instead, it includes the effects of chain ends, domain boundaries, disclinations, and network defects, which would all reduce the actual modulus in a highly oriented material from its theoretical value.

It is important to note that this analysis assumes that all mesogens are aligned at a single angle with respect to the magnetic field. Clearly from the X-ray data above this is not true. In reality, there is a distribution of mesogenic orientations, with many oriented parallel to the field and some oriented perpendicular to the field. The differences in orientation parameter result from changes in the distribution of these orientations. Nevertheless, the results do provide some insight into the nature of the enhancement in mechanical properties upon orientation in magnetic fields.

## Conclusions

This work has shown that it is possible to achieve high levels of orientation and substantial improvements in physical properties of liquid crystalline thermosets by curing in the presence of a magnetic field. At the highest field level studied, an orientation parameter for the smectic layer normals of 0.8 and a tensile modulus of 8.1 GPa is obtained. This is in contrast to a tensile modulus of 3.1 GPa for the unoriented material. It is apparent from the results, however, that the orientation process is a complex one. The orientation parameters from the outer reflection are considerably lower than those from the inner reflection. We have interpreted this as being due to the presence of domain boundaries and cross-links between the mesogens that result in regions of lower order than a smectic A phase. Thus, there is likely to be a complicated interplay among the presence of a high density of cross-links, the formation of a mesophase during the cure reaction, and the alignment induced by the magnetic field. Although the orientation process itself may be fairly complex, it nevertheless appears that the physical properties depend only on the final state of orientation in the material. The modulus vs orientation parameter data can be reasonably fit with a simple model based on performing a rotation operation on the modulus tensor, suggesting that the modulus is determined by the average orientation of the smectic structure.

**Acknowledgment.** Funding for this work was provided by the Department of Energy Advanced Industrial Materials Program and the National High Magnetic Field Laboratory. Partial funding to R.S.D. and S.M.S. was also provided by the NSF NYI program through the Division of Materials Research and through the NSF Academic Research Infrastructure program for X-ray equipment. Bruker Analytical X-ray Systems is acknowledged for technical support.

## References and Notes

(1) Sawyer, L. C.; Jaffe, M. *J. Mater. Sci.* **1986**, *21*, 1897.
(2) Plate, N. A.; Talroze, R. V.; Shibaev, V. P. *Makromol. Chem., Macromol. Symp.* **1987**, *12*, 203.
(3) Tal'roze, R. V.; Plate, N. A. In *Liquid-Crystal Polymers*; Plate, N. A., Ed.; Plenum Press: New York, 1993; p 303.
(4) Maret, G. In *Physical Phenomena at High Magnetic Fields*; Manousakis, E., Schlottman, P., Kumar, P., Bedell, K. S., Mueller, F. M., Eds.; Addison-Wesley Publishing Company: Redwood City, CA, 1991; p 458.
(5) Moore, R. C.; Denn, M. M. In *High Modulus Polymers, Approaches to Design and Development*; Zachariades, A. E., Porter, R. S., Eds.; Marcel Dekker: New York, 1990; p 169.
(6) Moore, R. C.; Denn, M. M.; Marrucci, G. *Polym. Mater. Sci. Eng.* **1985**, *52*, 84.
(7) Zhao, Y.; Lei, H. *Macromolecules* **1992**, *25*, 4043.
(8) Lembicz, F. *Polymer* **1991**, *32*, 2898.
(9) Maret, G.; Blumstein, A. *Mol. Cryst. Liq. Cryst.* **1982**, *88*, 295.
(10) Yamagishi, A.; Takeuchi, T.; Higashi, T.; Date, M. *J. Phys. Soc. Jpn.* **1989**, *58*, 2280.
(11) Wilkes, G. L. *J. Polym. Sci.: Polym. Lett. Ed.* **1972**, *10*, 935.
(12) Stupp, S. I.; Moore, J. S. *Polym. Mater. Sci. Eng.* **1986**, *54*, 136.
(13) Kishi, R.; Sisido, M.; Tazuke, S. *Macromolecules* **1990**, *23*, 3868.
(14) Oulyadi, H.; Laupretre, F.; Monnerie, L.; Mauzac, M.; Richard, H.; Gasparoux, H. *Macromolecules* **1990**, *23*, 1965.
(15) Piskunov, M.; Kostromin, S. G.; Stroganov, L. B.; Shibaev, V. P.; Plate, N. A. *Makromol. Chem., Rapid Commun.* **1982**, *3*, 443.
(16) Volino, F.; Martins, A. F.; Blumstein, R. B.; Blumstein, A. *J. Phys.—Lett.* **1981**, *42*, L-305.
(17) Rigbi, Z.; Mark, J. E. *J. Polym. Sci.: Polym. Phys. Ed.* **1985**, *23*, 1267.

(18) Aviram, A. *J. Polym. Sci.: Polym. Lett. Ed.* **1976**, *14*, 757.
(19) Roche, P.; Zhao, Y. *Macromolecules* **1995**, *28*, 2819.
(20) Martin, C.; Kramer, H.; Johner, C.; Weyerich, B.; Biegel, J.; Deike, R.; Hagenbuchle, M.; Weber, R. *Macromolecules* **1995**, *28*, 3175.
(21) Williams, D. R. M.; Halperin, A. *Macromolecules* **1993**, *26*, 2025.
(22) Wagner, N. J.; Walker, L. M. *Macromolecules* **1994**, *27*, 5979.
(23) Anwer, A.; Windle, A. H. *Polymer* **1993**, *34*, 3347.
(24) Hudson, S. D.; Thomas, E. L. *Polym. Prepr.* **1990**, *31*, 379.
(25) Yamagishi, A.; Takeuchi, T.; Higashi, T.; Date, M. *Physica B* **1990**, *164*, 222.
(26) Iizuka, E. *J. Appl. Polym. Sci.: Appl. Polym. Symp.* **1985**, *41*, 131.
(27) Fuhrmann, K.; Dries, T.; Fischer, E. W.; Ballauff, M. *J. Polym. Sci., Part B: Polym. Phys.* **1992**, *30*, 1199.
(28) Iizuka, E.; Kondo, Y. *Mol. Cryst. Liq. Cryst.* **1979**, *51*, 285.
(29) Moore, J. S.; Stupp, S. I. *Macromolecules* **1987**, *20*, 282.
(30) Barclay, G. G.; Ober, C. K.; Papathomas, K. I.; Wang, D. W. *Macromolecules* **1992**, *25*, 2947.
(31) Barclay, G. G.; McNamee, S. G.; Ober, C. K.; Papathomas, K. I.; Wang, D. W. *J. Polym. Sci., Part A: Polym. Chem.* **1992**, *30*, 1845.
(32) Ober, C. K.; Barclay, G. G. *Mater. Res. Soc. Symp. Proc.* **1991**, *227*, 281.
(33) Jahromi, S.; Kuipers, W. A. G.; Norder, B.; Mijs, W. J. *Macromolecules* **1995**, *28*, 2201.
(34) Litt, M. H.; Whang, W.-T.; Yen, K.-T.; Qian, X.-J. *J. Polym. Sci., Part A: Polym. Chem.* **1993**, *31*, 183.
(35) Melissaris, A. P.; Litt, M. H. *Macromolecules* **1994**, *27*, 2675.
(36) Melissaris, A. P.; Sutter, J. K.; Litt, M. H.; Scheiman, D. A.; Schuerman, M. A. *Macromolecules* **1995**, *28*, 860.
(37) Hikmet, R. A. M.; Broer, D. J. *Polymer* **1991**, *32*, 1627.
(38) Shiota, A.; Ober, C. K. *J. Polym. Sci., Part B: Polym. Phys.* **1998**, *36*, 31.
(39) Carfagna, C.; Amendola, E.; Giamberini, M. In *Liquid Crystalline Polymers: Proceedings of the International Workshop on Liquid Crystalline Polymers*; Carfagna, C., Ed.; Pergamon Press: Oxford, U.K., 1994; pp 69−85.
(40) Carfagna, C.; Amendola, E.; Giamberini, M. *Compos. Struct.* **1994**, *27*, 37.
(41) Su, W.-F. A. *J. Polym. Sci., Part A: Polym. Chem.* **1993**, *31*, 3251.
(42) Hoyle, C. E.; Watanabe, T.; Brister, E.; Whitehead, J. *Polym. Prepr.* **1993**, *34*, 703.
(43) Jahromi, S. *Macromolecules* **1994**, *27*, 2804.
(44) Hoyle, C. E.; Watanabe, T.; Whitehead, J. B. *Macromolecules* **1994**, *27*, 6581.
(45) Earls, J. D.; Hefner, R. E.; Puckett, P. M. U.S. Patent 5,270,405, 1993.
(46) Hoyt, A. E.; Benciewicz, B. C. *J. Polym. Sci.: Part A: Polym. Chem.* **1990**, *28*, 3417.
(47) Douglas, E. P.; Langlois, D. A.; Benicewicz, B. C. *Chem. Mater.* **1994**, *6*, 1925.
(48) Mallon, J. J.; Adams, P. M. *J. Polym. Sci.: Part A: Polym. Chem.* **1993**, *31*, 2249.
(49) Flory, P. J. *Proc. R. Soc. London, A* **1956**, *234*, 73.
(50) Lin, Q.; Yee, A. F.; Earls, J. D.; Hefner, R. E., Jr.; Sue, H.-J. *Polymer* **1994**, *35*, 2679.
(51) de Gennes, P. G.; Prost, J. *The Physics of Liquid Crystals*; Clarendon Press: Oxford, U.K., 1993.
(52) Marinov, Y.; Simova, P. *Liq. Cryst.* **1992**, *12*, 657.
(53) Beekmans, F.; de Boer, F. *Macromolecules* **1996**, *29*, 8726.
(54) Hanabusa, K.; Hashimoto, M.; Kimura, M.; Koyama, T.; Shirai, H. *Macromol. Chem. Phys.* **1996**, *197*, 1853.
(55) Miyano, K. J. *Chem. Phys.* **1978**, *69*, 4807.
(56) Kruk, G.; Vij, J. K.; Ringsdorf, H. *Supramol. Sci.* **1995**, *2*, 51.
(57) Jen, S.; Clark, N. A.; Pershan, P. S.; Priestley, E. B. *Phys. Rev. Lett.* **1973**, *31*, 1552.
(58) Walker, L. M.; Kernick, W. A.; Wagner, N. J. *Macromolecules* **1997**, *30*, 508.
(59) Crevecoeur, G.; Groeninckx, G. *Polym. Compos.* **1992**, *13*, 1266.
(60) Hongladarom, K.; Ugaz, V. M.; Cinader, D. K.; Burghardt, W. R.; Quintana, J. P.; Hsiao, B. S.; Dadmun, M. D.; Hamilton, W. A.; Butler, P. D. *Macromolecules* **1996**, *29*, 5346.
(61) Alexander, L. E. *X-ray Diffraction Methods in Polymer Science*; John Wiley and Sons: New York, 1969.
(62) Balta-Calleja, F. J. *X-ray Scattering of Synthetic Polymers*; Elsevier: New York, 1989.
(63) Masao, K. *X-ray Diffraction by Polymers*; Elsevier: New York, 1972.
(64) Warren, B. E. *X-ray Diffraction*; Dover Publications: New York, 1990.
(65) Klug, H. P. *X-ray Diffraction Procedures for Polycrystalline and Amorphous Materials*; John Wiley and Sons: New York, 1974.
(66) Lafrance, C. P.; Pézolet, M.; Prud'homme, R. E. *Macromolecules* **1991**, *24*, 4948.
(67) Reeves, N. J.; Evans, J. S. *J. Phys. Chem.* **1996**, *100*, 17297.
(68) Moon, H. S.; Park, J. K.; Liu, J. U. *J. Appl. Polym. Sci.* **1996**, *59*, 489.
(69) Bruggeman, A.; Buijs, J. A. H. *Polymer* **1996**, *37*, 5639.
(70) Andersson, H.; Sahlen, F.; Trollsas, M.; Gedde, U. W.; Hult, A. *J. Macromol. Sci.—Pure Appl. Chem.* **1996**, *A33*, 1427.
(71) Holter, D.; Frey, H.; Mulhaupt, R.; Klee, J. E. *Macromolecules* **1996**, *29*, 7003.
(72) Lafrance C. P., Prud'homme, R. E.; Brisson, J. *Polymer* **1996**, *37*, 1509.
(73) Yu, T. H.; Wilkes, G. L. *Polymer* **1996**, *37*, 4675.
(74) Lafrance, C. P.; Nabet, A.; Prud'homme, R. E.; Pézolet, M. *Can. J. Chem.* **1995**, *73*, 1497.
(75) Anmer, A.; Windle, A. H. *Polymer* **1991**, *32*, 103.
(76) Lin, Q.; Yee, A. F.; Sue, H.-J.; Earls, J. D.; Hefner, R. E., Jr. *J. Polym. Sci., Part B: Polym. Phys.* **1997**, *35*, 2363.
(77) Kurdikar, D. L.; Boots, H. M. J.; Peppas, N. A. *Macromolecules* **1995**, *28*, 5632.
(78) Shiota, A.; Ober, C. K. *Macromolecules* **1997**, *30*, 4278.
(79) Körner, H.; Shiota, A.; Bunning, T. J.; Ober, C. K. *Science* **1996**, *272*, 252.
(80) Lees, J. K. *Polym. Eng. Sci.* **1968**, *8*, 186.
(81) Holliday, L.; Ward, I. M. In *Structure and Properties of Oriented Polymers*; Ward, I. M., Ed.; John Wiley & Sons: New York, 1975; pp 30−31.
(82) Ide, Y.; Chung, T. *J. Macromol. Sci.—Phys.* **1984−85**, *B23*, 497.
(83) Smith, M. E.; Douglas, E. P.; Benicewicz, B. C.; Earls, J. D.; Priester, R. D., Jr. *Mater. Res. Soc. Proc.* **1996**, *425*, 167.

MA980058M